Applied Physics Letters ARTICLE pubs.aip.org/aip/apl

Epitaxial high-K barrier AlBN/GaN HEMTs

Cite as: Appl. Phys. Lett. **126**, 112906 (2025); doi: 10.1063/5.0235294
Submitted: 26 August 2024 · Accepted: 19 February 2025 ·
Published Online: 18 March 2025

Chandrashekhar Savant,[1,a)] Thai-Son Nguyen,[1] Kazuki Nomoto,[2] Saurabh Vishwakarma,[3] Siyuan Ma,[1] Akshey Dhar,[1] Yu-Hsin Chen,[1] Joseph Casamento,[4] David J. Smith,[5] Huili Grace Xing,[1,2,6] and Debdeep Jena[1,2,6,7]

AFFILIATIONS

[1]Department of Materials Science and Engineering, Cornell University, Ithaca, New York 14853, USA
[2]School of Electrical and Computer Engineering, Cornell University, Ithaca, New York 14853, USA
[3]School for Engineering of Matter, Transport and Energy, Arizona State University, Tempe, Arizona 85287, USA
[4]Department of Materials Science and Engineering, Massachusetts Institute of Technology, Cambridge, Massachusetts 02139, USA
[5]Department of Physics, Arizona State University, Tempe, Arizona 85287, USA
[6]Kavli Institute at Cornell for Nanoscale Science, Cornell University, Ithaca, New York 14853, USA
[7]School of Applied and Engineering Physics, Cornell University, Ithaca, New York 14853, USA

[a)]**Author to whom correspondence should be addressed:** cps259@cornell.edu

ABSTRACT

We report a polarization-induced 2D electron gas (2DEG) at an epitaxial AlBN/GaN heterojunction grown on a SiC substrate. Using this 2DEG in a long conducting channel, we realize ultra-thin barrier AlBN/GaN high electron mobility transistors that exhibit current densities > 0.25 A/mm, clean current saturation, a low pinch-off voltage of -0.43 V, and a peak transconductance of ~ 0.14 S/mm. Transistor performance in this preliminary realization is limited by the contact resistance. Capacitance–voltage measurements reveal that introducing $\sim 7\%$ B in the epitaxial AlBN barrier on GaN boosts the relative dielectric constant of AlBN to $\varepsilon_r^{AlBN} \sim 16$, higher than the AlN dielectric constant of $\varepsilon_r^{AlN} \sim 9$. Epitaxial high-K barrier AlBN/GaN HEMTs can thus extend performance beyond the capabilities of current GaN transistors.

High electron mobility transistors (HEMTs) using the semiconductor GaN achieve high-voltage and high-frequency operation due to the wide bandgap and polarization fields in epitaxial heterostructures that give high electron velocities, breakdown fields, mobile carrier densities, and electron mobility.[1–4] The 2D electron gas (2DEG) channel induced at the AlGaN/GaN heterojunction by polarization discontinuity offers six times a higher electron mobility than Si MOSFETs.[2,4,5] GaN HEMTs offer a compelling energy efficiency advantage in computation by conditioning and delivering power to silicon microprocessors via heterogeneous integration in a manner unmatched by any other semiconductor.[6] GaN HEMT RF power amplifiers add communication capability to silicon.[7–10] Today's state-of-the-art HEMTs for power electronics and RF applications utilize AlGaN barrier layers on a GaN channel grown epitaxially on silicon, SiC, or sapphire substrates.[11–13]

Developed in the early 2000s and deployed in the past decade, such conventional AlGaN/GaN heterostructures are approaching their performance limits in HEMTs.[11,14] The dielectric constant ε_r of typical AlGaN barriers with Al mole fraction ~ 0.3 is ~ 8.4–9, and the energy bandgap is ~ 4.2 eV.[15] The modest dielectric constant, energy bandgap (and band offset), and tensile strain present in AlGaN now limit the HEMT performance. Similar limitations of barrier properties of SiO_2 in Si CMOS in the early 2000s were solved by introducing high-K dielectric HfO_2 barriers in 2006, enhancing device performance and enabling Moore's law scaling.[16] In HfO_2, ferroelectricity was later discovered by doping with Zr, Si, or La, enabling FerroFET memories as a bonus.[16–18] Nitride HEMTs now need hi-K barriers analogous to $Hf_{0.5}Zr_{0.5}O_2$ (HZO) for silicon, but which must simultaneously be ultrawide bandgap and epitaxial to provide the polarization-induced conductive channels.

The investigation of alternate barriers for GaN HEMTs, such as lattice-matched AlInN and binary AlN, has yielded encouraging results, but the dielectric constant of these barriers is still modest. Over the last few years, AlScN has emerged as an interesting option, thanks to the discovery of ferroelectricity,[19] high-K dielectric properties,[20] and lattice-matching to GaN.[21–23] Although AlScN barrier RF and mm-wave GaN HEMTs[24–26] and FerroHEMTs[27,28] have been demonstrated, the semiconductor community is addressing challenges of

chemical oxidation,[29,30] energy bandgap reduction,[31] and structural instabilities and phase separation in high Sc-containing AlScN.

Ferroelectric[32–35] and high-K dielectric properties[32] were recently reported in AlBN layers. The large energy bandgap and chemical inertness make AlBN barriers worth investigating as an alternate barrier material for high-voltage, high-temperature GaN transistors. Here, we report the epitaxial integration of the AlBN gate barrier on the GaN platform and the realization of AlBN/GaN HEMTs. We grew AlBN/GaN heterostructures by MBE on 3-in. diameter 6H-SiC wafers and observed polarization-induced 2DEGs. We then fabricated AlBN/GaN HEMTs using alloyed metallic Ta/Al/Ni/Au Ohmic "claw" contacts and standard Schottky gates and observed encouraging transistor characteristics. We find that the addition of ∼7% B boosts the dielectric constant of AlN by nearly two times to $\varepsilon_r^{AlBN} = 16$ at 2 MHz at 20 °C. By measuring the capacitance–voltage characteristics of thin AlBN barrier/GaN heterostructure-based MIS capacitors in several devices and at various frequencies, we confirmed that epitaxial AlBN on GaN is a robust, hi-K epitaxial dielectric that simultaneously provides polarization-induced conductive channels.

Figure 1(a) schematically shows the AlBN/GaN HEMT heterostructure realized by MBE for this study. We first grew a ∼125-nm AlN nucleation layer on the SiC substrate, starting with a nitrogen-rich AlN layer with III/V ratio ∼0.7 to capture surface impurities and block Si diffusion and then transitioned to metal-rich AlN with III/V ∼1.1 to promote smooth AlN growth.[36] We then grew a 600-nm-thick unintentionally doped (UID) GaN layer under metal-rich conditions with a III/V ratio >1, followed by ∼2.2-nm epitaxial wurtzite phase AlBN barrier film at a III/V flux ratio of 0.7. Nitrogen-rich growth conditions are necessary to grow AlBN because N has a thermodynamic preference to bond to Al rather than to B.[37] We then deposited a 2-nm UID GaN cap to protect the barrier layer from surface contamination.

Figure 1(b) shows an AFM micrograph of a dislocation-mediated, yet smooth surface morphology of an as-grown AlBN/GaN heterostructure with 0.62-nm rms roughness over a $10 \times 10\ \mu m^2$ scan area. Figure 1(c) shows the streaky RHEED pattern of AlBN films along the[11–20] zone axis observed during MBE growth, confirming that the AlBN film is epitaxial and of wurtzite phase. Figure 1(d) shows a cross-sectional HRTEM image of the GaN/AlBN/UID GaN heterostructure up to ∼40-nm depth from the surface. AlBN is in lighter contrast, sandwiched between the darker GaN cap and the UID GaN layers. The micrograph shows the AlBN and GaN layers are crystalline. The AlBN/GaN interfaces are not as smooth as typical AlN/GaN interfaces, but the thin AlBN layer is continuous with slightly varying thickness. The fast Fourier transform (FFT) pattern of the region marked by the square red box in the inset of Figure 1(d) confirms the wurtzite phase of AlBN, GaN, and the epitaxial relationship between the layers. The smearing of low-frequency FFT spots due to the slight difference in lattice parameters between GaN and AlBN also confirms the presence of the AlBN layer. ToF-SIMS composition depth profile of ^{11}B, Al, and Ga species in Fig. 1(e) verifies the presence of boron in the AlBN layer. We determined the B/(Al + B) ratio in the AlBN barrier layer to be 7.4% by XPS measurements. XRR measurements confirm ∼2-nm thickness for the GaN cap and ∼2.2-nm thickness for the AlBN barrier. TEM micrographs of the AlBN barrier sample further confirm the film thicknesses of the GaN cap to be 2-nm and the AlBN layer to be 2.2-nm.

Figure 2 shows the results of temperature-dependent Hall effect measurements performed on diced $1 \times 1\ cm^2$ samples from the center region of the as-grown 3-in. diameter AlBN/GaN heterostructure wafer using a van der Pauw geometry with indium contacts. We obtained these data by varying the temperature from 10 to 320 K in a Lakeshore Hall measurement system at 1 T. At 300 K, we observe a polarization-induced 2DEG sheet concentration $N_s = 9.25 \times 10^{12}$ /cm^2, electron mobility $\mu = 524\ cm^2/V{\cdot}s$, and a sheet resistance $R_s = 1290\ \Omega/sq$ in the AlBN/GaN heterostructure. We observe < 6% decrease in the sheet density as temperature decreases from 320 to 10 K, indicating minimal carrier freeze out. The low-temperature plateauing of the sheet carrier density, electron mobility, and sheet resistance confirm the presence of a typical 2DEG.[26] We observe the 2DEG across the large 3-in. wafer, with sheet density N_s between

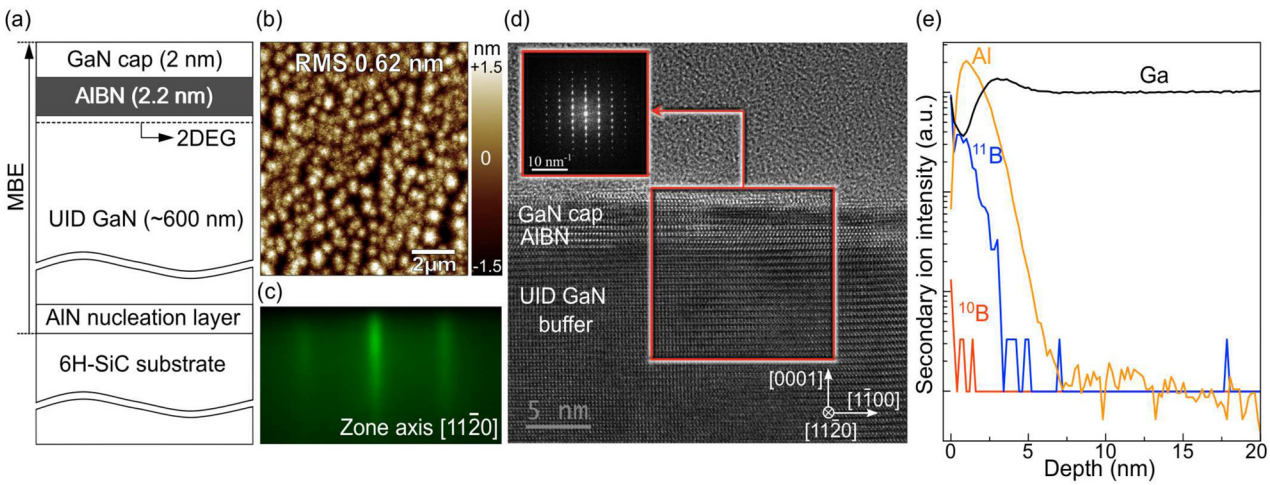

FIG. 1. (a) Epitaxial AlBN/GaN heterostructure indicating a polarization-induced 2DEG at the heterojunction, (b) AFM micrograph, (c) RHEED pattern along[11–20] the zone axis, and (d) HRTEM micrograph of AlBN/GaN heterostructure. Inset shows FFT analysis of red marked region indicating wurtzite phase. (e) Composition-depth profiles of Al, Ga, ^{11}B, and ^{10}B species as measured by ToF-SIMS.

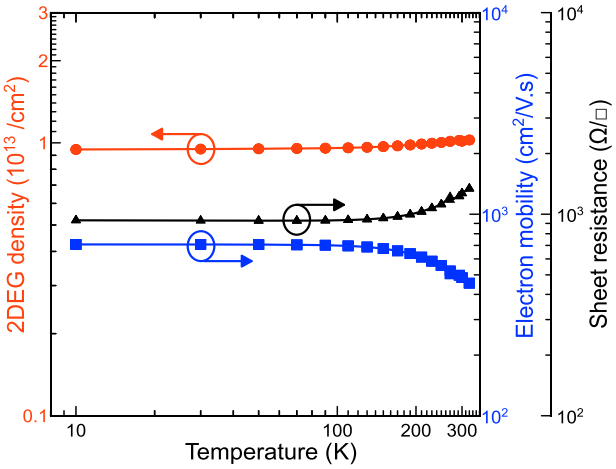

FIG. 2. Temperature-dependent Hall effect measurement data showing electron density, mobility, and sheet resistance from 320 to 10 K confirming 2DEG properties in the AlBN/GaN heterostructure. The measurement was performed with indium dots on the center 1 × 1 cm^2 sample diced from the 3-in. diameter wafer.

7.1–9.3 × 10^{12}/cm^2. We re-measured the Hall data on an as-grown sample 16 months after the MBE growth to find a nearly unchanged sheet density, mobility, and sheet resistivity. The 2DEG density we measure in the 2.2-nm AlBN/GaN heterostructure is lower than the sheet density of 2.08 × 10^{13}/cm^2 in a comparable 2-nm AlN/GaN heterostructure[27] due to the higher dielectric constant of AlBN relative to AlN.

In Fig. 3(a), we have outlined the process flow used to realize the HEMTs shown in Figs. 3(b) and 3(c) from 1 × 1 cm^2 samples diced from the center of the 3-in. diameter wafer. Dry BCl_3 inductively coupled plasma (ICP) was performed for device isolation and to simultaneously create trenches for metal sidewall contacts to the 2DEG. We defined the source/drain regions with a SiO_2/Cr hard mask and deposited Ta/Al/Ni/Au (20/150/50/50-nm) metal stack[38,39] using e-beam evaporation for source/drain contacts, and annealed the stack at 830 °C for 65 s in N_2 ambient. We deposited a 30/220-nm Ni/Au gate metal stack directly on the sample surface and defined the gate lengths L_g by photolithography. Figure 3(b) shows the AlBN/GaN HEMT device cross section schematic with the alloyed claw source/drain contacts to the 2DEG channel. Figure 3(c) shows the SEM image of a fully processed HEMT viewed from the top. All HEMTs reported in this study have a source-to-drain spacing $L_{sd} = 2.3\,\mu$m, device-width $W = 50\,\mu$m, and a rectangular gate placed in the middle of the source-to-drain spacing with a gate length $L_g = 1.3\,\mu$m.

We repeated 300 K Hall effect measurements on processed van der Pauw patterns after device fabrication. As shown in Fig. 3(d), we measured 2DEG sheet densities $N_s = 1.41$–1.48×10^{13}/cm^2, mobilities $\mu = 700$–707 cm^2/V s, and sheet resistances $R_s = 598$–630 Ω/sq across different dies with alloyed contacts. The higher mobility and sheet density and consequently lower sheet resistance after device processing compared to the as-grown data, presumably due to annealing steps during the device processing, need to be understood better in the future.[40–42]

We assessed buffer leakage through the UID GaN layer by removing the top 60-nm of the MBE-grown AlBN/GaN heterostructure to remove the active region of some HEMTs by BCl_3 ICP etching, and found low leakage currents of ∼0.1 nA/mm at 20 V for 5-μm spacing between two alloyed contacts indicating its high resistivity. Transfer length measurements on the AlBN/GaN heterostructure devices revealed nonlinear IV characteristics with Schottky behavior of unoptimized alloyed contacts. The measured contact resistance R_c is ∼1.44 Ω · mm and drops to below 1Ω · mm when the current exceeds 150 mA/mm. The specific contact resistance is ∼5 × 10^{-6} Ω · cm^2 and approaches ∼3.6 × 10^{-6} Ω · cm^2 at 150 mA/mm.

Figures 4(a) and 4(b) show the log and linear scale HEMT transfer characteristics revealing I_{on}/I_{off} ∼7 × 10^3 limited by gate leakage. We observe sharp pinch-off characteristics with a low threshold

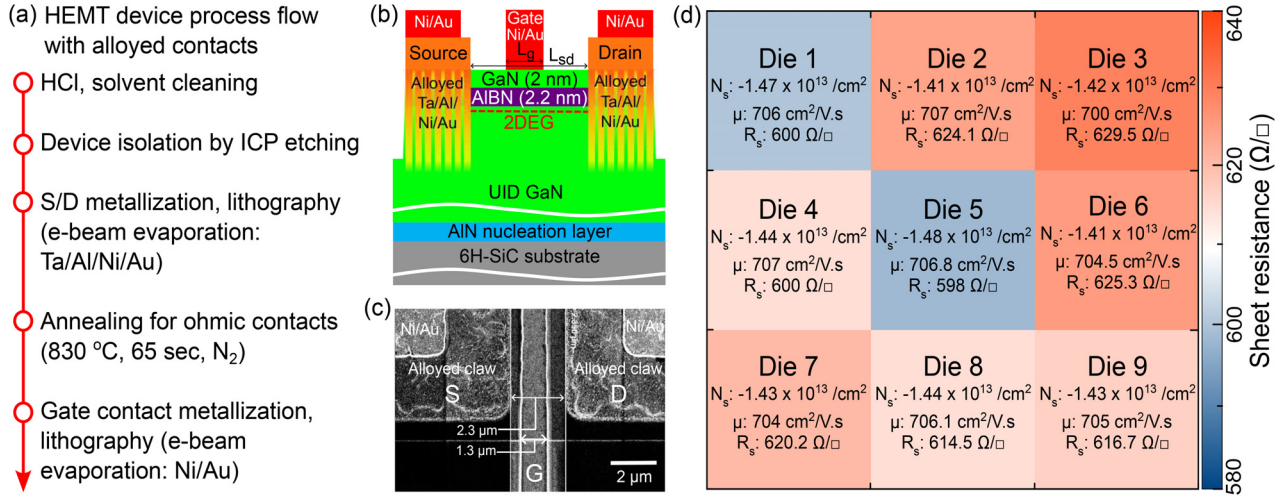

FIG. 3. (a) The device process flow of group III-nitride HEMTs with alloyed contacts and (b) schematic cross section of ∼7% B containing AlBN barrier GaN HEMT showing the alloyed contacts, gate, and channel regions. (c) Scanning electron microscope (SEM) image of a processed HEMT showing source (S), drain (D), and gate (G) regions. (d) Room temperature Hall-effect data for ∼7% B containing AlBN barrier GaN HEMT measured after device processing.

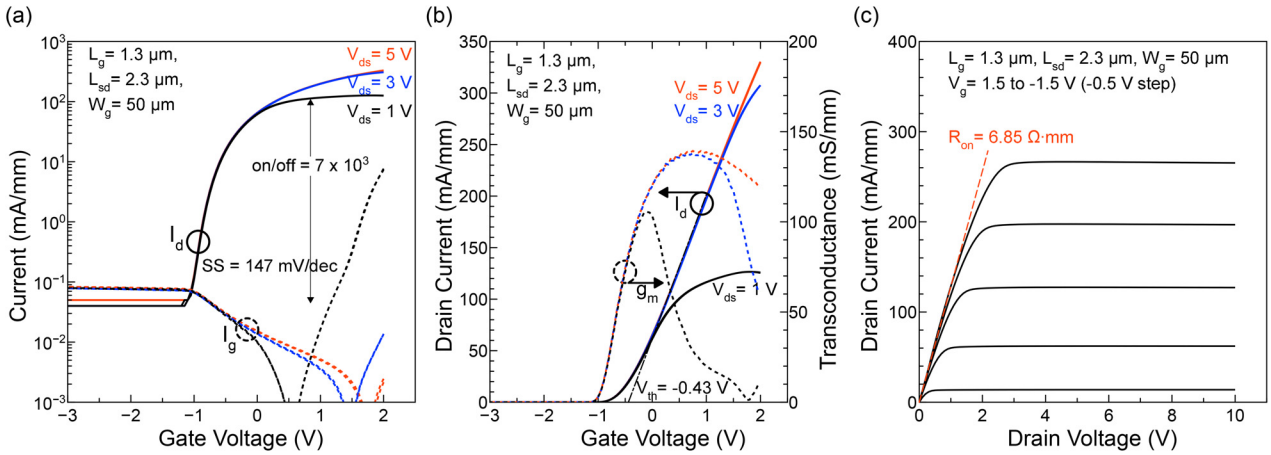

FIG. 4. (a) Measured characteristics of the GaN HEMT with AlBN barrier with ∼7% B: (a) log scale and (b) and linear scale transfer characteristics showing an on/off ratio exceeding three orders and transconductance vs V_{gs} showing a peak transconductance of 139 mS/mm and (d) output characteristics showing on resistance $R_{on} = 6.8\Omega$ mm with repeatable current saturation and a maximum drain current I_d of 280 mA/mm at a gate voltage of $V_{gs} = 1.5$ V.

voltage $V_{th} = -0.43$ V at different drain biases $V_{ds} = 1$, 3, and 5 V, suggesting minimal drain-induced barrier lowering (DIBL), with a minimum sub-threshold slope (SS) of 147 mV/decade and peak extrinsic transconductance $g_m^{ext} = 139$ mS mm^{-1}. Figure 4(c) shows the HEMT output characteristics with clean current saturation of the drain current I_d, its control with gate bias V_{gs} from on-state to pinch-off. We measure a transistor on-resistance $R_{on} = 6.85\,\Omega$ mm, and a saturation drain current $I_d^{sat} = 266$ mA/mm at $V_{gs} = 1.5$ V. The transistor characteristics, currently limited by contact resistance, exhibit a low threshold voltage.

We measured capacitance–voltage (C-V) characteristics on metal-insulator-semiconductor (MIS) capacitors of GaN-cap/AlBN/GaN structure using circular Ni/Au pads with 20, 40, and 80 μm diameters as top electrodes and the 2DEG accessed using alloyed contacts as the bottom electrode. Figure 5 shows the measured C–V characteristics of the 2-nm GaN-cap/2.2-nm AlBN/GaN heterostructure-based MIS capacitor at 2 MHz AC at 20 °C. The solid line shows the calculated C-V characteristics using a self-consistent 1D Schrödinger–Poisson solution.[43] Parameters used in the simulation are the relative dielectric constant of GaN $\varepsilon_r^{GaN} = 10.4$, a polarization discontinuity of 11.8 μ C/cm^2,[44] at the AlBN/GaN heterojunction, an AlBN bandgap of $E_g^{AlBN} = 6.1$ eV, and an AlBN/GaN conduction band offset $\Delta E_c = 2.234$ eV, and the measured thicknesses of the UID GaN cap layer of 2 nm, the AlBN barrier layer of 2.2 nm using the high-resolution transmission electron microscope images and x-ray reflectivity spectra. From the simulation, the relative dielectric constant of AlBN is estimated to be $\varepsilon_r^{AlBN} \sim 16$, compared to $\varepsilon_r^{AlN} \sim 9$ for AlN. The sharp decrease in capacitance at negative voltage when the 2DEG depletes is consistent with the HEMT transfer characteristics seen in Fig. 4(b).

By performing the C–V measurements at 0.1, 0.5, 1, and 2 MHz frequencies (see the supplementary material), we found the AlBN capacitance to be consistently higher than AlN, with the value decreasing slightly at high frequencies for both AlBN and AlN-based devices. This indicates a negligible effect of the space charge polarization and that the ionic and dipole polarization likely plays a role in enhancing the dielectric constant of AlBN. Theoretical studies indicated an enhancement in the dielectric constant of AlN with B incorporation due to increased ionicity from a change in the local charge distribution, a decrease in structural stability, and/or softening of IR-active phonon modes.[45] The higher dielectric constant seen in our MBE-grown AlBN thin films is consistent with the high-K dielectric nature reported in thick sputter-deposited AlBN films.[32] A slight difference in the observed dielectric constants between MBE-grown and sputter-deposited AlBN films could be due to different substrates and inherently different growth dynamics offered by MBE and sputtering. The

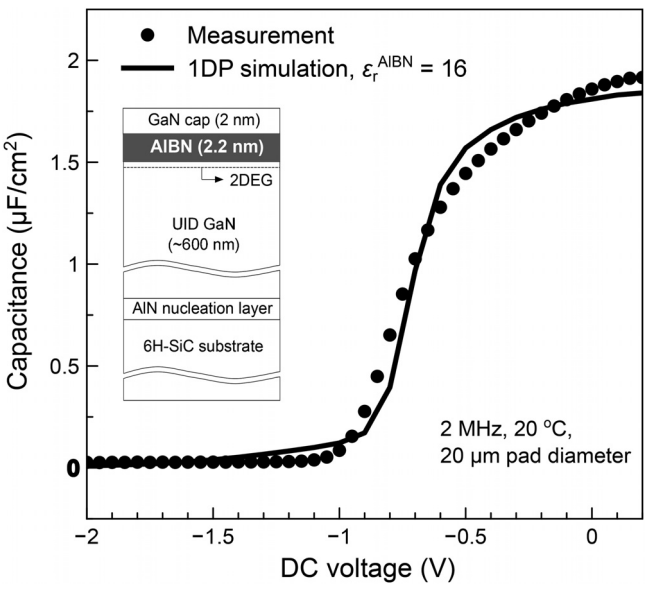

FIG. 5. Measured CV characteristics (points) of 2-nm GaN cap/2.2-nm AlBN/GaN-based metal-insulator-semiconductor (MIS) capacitor at 2 MHz, 20 °C overlaid with 1D Schrödinger Poisson simulated CV characteristics indicating that the dielectric constant of the AlBN barrier is $\varepsilon_r^{AlBN} \sim 16$.

epitaxial AlBN films in this work were grown on polar GaN semiconducting substrates, whereas the AlBN films reported by Hayden *et al.* were sputter deposited on nonpolar metallic tungsten layers.[32] Different strain conditions in the AlBN films grown on GaN by MBE vs on metal by sputtering can impact the respective dielectric constants. The growth dynamics, resulting crystallinity, and chemical purity differ between MBE and sputter-deposition. Owing to the ultrahigh vacuum nature of MBE, elemental purity of sources, and minimum substrate damage from the low kinetic energies of evaporated molecular beams, MBE growth on epitaxial substrates yields films of high crystal quality, chemical purity, and controlled stoichiometry.[46] These factors can affect the local dipole moments and distributions, affecting the measured dielectric constant of the AlBN films grown by different methods and on different substrates. Regardless, the high-K nature of AlBN films over that of AlN films is unambiguous. The above-mentioned results provide strong evidence that AlBN on GaN is an epitaxial high-K dielectric that can simultaneously provide polarization-induced 2DEGs and appropriate insulating properties to serve as the gate barrier of AlBN/GaN HEMTs.

Thus, boron-containing AlBN joins other transition or rare-earth metal high-K wurtzite nitrides such as AlScN, AlYN, AlLaN, and AlLuN.[19,32,47–49] The energy bandgap of AlN does not shrink substantially upon B substitution because the energy bandgaps of BN variants (5.96 eV for h-BN, 6.4 eV for c-BN, and 6.84 eV for wurtzite-BN) are similar to AlN.[32,45,50–53] In contrast, the energy bandgaps of the binary nitrides of Sc, Y, La, and Lu are substantially smaller than AlN.[28,54–59] UV-visible spectroscopic measurements of thick AlBN MBE-grown films indicate a slight reduction of AlN bandgap from 6.1 eV to 6.0 eV with ∼7% B incorporation, compared to 5.77 eV for ∼7% Sc incorporation.[31] Thus, the ultrawide bandgap of AlBN is expected to maintain a larger breakdown voltage than other hi-K nitride alternatives.

The route to incorporation of the non-transition group metal B in AlN differs from the group III transition metal Sc[19,60] (and its variants such as Y[47,59] or La[48,57]) in *four* essential ways: (1) the B-N chemical bonds do not involve d-orbitals—the competing crystal structure of BN is layered hexagonal with sp^2 bonds, and the less stable cubic and hexagonal wurtzite variants of BN have sp^3 bonds;[50] (2) the d_{33} piezoelectric coefficient does not increase (it slightly *decreases* in AlBN compared to AlN);[50,52] (3) since B atom is lighter than Al, the thermal conductivity of AlBN, though lower than AlN due to alloy scattering of phonons, is expected to be higher than for the heavier transition metal Sc, Y, or La alloys with AlN;[49,61,62] and (4) AlBN is expected to be more resistant to oxidation compared to AlScN and other transition/rare-earth metal-based nitrides.[29,30] Thus, AlBN has the potential to be an electronically, thermally, and chemically robust high-K dielectric suited for high temperature and harsh environment RF, power, and memory devices based on GaN.

In summary, the observations reported here about (1) the epitaxial growth of AlBN/GaN heterostructures, (2) the observation of polarization-induced 2DEG channels at the AlBN/GaN heterojunction, (3) the process compatibility to form HEMTs with ultrathin AlBN barriers, and (4) the observation of high-K dielectric properties of AlBN barrier layers offer significant hope for surpassing limitations imposed by AlGaN barriers in current GaN HEMT technology for power electronics and RF/mm-wave applications of this revolutionary semiconductor family.

See the supplementary material for the 300 K Hall effect measurements map of a 3-in. diameter wafer with sheet resistivity, electron mobility, and 2DEG sheet density, with buffer leakage measurement and CV measurements on multiple devices with different top electrode diameters at different measurement frequencies confirming the high-K dielectric nature of the MBE AlBN film over the control AlN film.

This work was supported in part by the Ultra Materials for a Resilient Energy Grid (epitaxial growth, microscopy, and characterization), an Energy Frontier Research Center funded by the U.S. Department of Energy, Office of Science, Basic Energy Sciences under Award No. DE-SC0021230, in part by SUPREME, one of seven centers in JUMP 2.0, a Semiconductor Research Corporation (SRC) program sponsored by DARPA (device fabrication) and in part by ARO Grant No. W911NF2220177 (device characterization). This work used the Cornell Center for Materials Research (CCMR) Shared Facilities, which are supported by the NSF MRSEC program (No. DMR-1719875). The authors acknowledge the use of the Cornell NanoScale Facility (CNF), a member of the National Nanotechnology Coordinated Infrastructure (NNCI), which is supported by the National Science Foundation (NSF Grant No. NNCI-2025233).

AUTHOR DECLARATIONS

Conflict of Interest

The authors have no conflicts to disclose.

Author Contributions

Chandrashekhar Savant, Thai-Son Nguyen, and Kazuki Nomoto contributed equally to this work.

Chandrashekhar Savant: Conceptualization (lead); Data curation (equal); Formal analysis (equal); Investigation (equal); Methodology (lead); Resources (equal); Software (equal); Validation (equal); Writing – original draft (lead); Writing – review & editing (equal). **Thai-Son Nguyen:** Data curation (equal); Formal analysis (equal); Investigation (equal); Software (equal); Validation (equal); Writing – review & editing (supporting). **Kazuki Nomoto:** Conceptualization (equal); Data curation (equal); Formal analysis (equal); Methodology (equal); Validation (equal); Writing – review & editing (supporting). **Saurabh Vishwakarma:** Data curation (supporting); Investigation (supporting); Writing – review & editing (supporting). **Siyuan Ma:** Software (supporting). **Akshey Dhar:** Methodology (supporting); Software (supporting). **Yu-Hsin Chen:** Methodology (supporting); Software (supporting). **Joseph Casamento:** Project administration (supporting); Validation (supporting). **David J. Smith:** Project administration (supporting); Resources (supporting); Supervision (supporting); Writing – review & editing (supporting). **Huili Grace Xing:** Conceptualization (supporting); Funding acquisition (equal); Investigation (equal); Project administration (equal); Resources (equal); Supervision (equal). **Debdeep Jena:** Conceptualization (equal); Funding acquisition (equal); Investigation (equal); Methodology (equal); Project administration (lead); Resources (equal); Supervision (lead); Writing – original draft (supporting); Writing – review & editing (equal).

DATA AVAILABILITY

The data that support the findings of this study are available from the corresponding author upon reasonable request.

REFERENCES

[1]M. A. Khan, J. Kuznia, J. Van Hove, N. Pan, and J. Carter, "Observation of a two-dimensional electron gas in low pressure metalorganic chemical vapor deposited GaN-$Al_xGa_{1-x}N$ heterojunctions," Appl. Phys. Lett. **60**, 3027–3029 (1992).

[2]O. Ambacher, J. Smart, J. Shealy, N. Weimann, K. Chu, M. Murphy, W. Schaff, L. Eastman, R. Dimitrov, L. Wittmer *et al.*, "Two-dimensional electron gases induced by spontaneous and piezoelectric polarization charges in N-and Ga-face AlGaN/GaN heterostructures," J. Appl. Phys. **85**, 3222–3233 (1999).

[3]M. Asif Khan, A. Bhattarai, J. Kuznia, and D. Olson, "High electron mobility transistor based on a GaN-$Al_xGa_{1-x}N$ heterojunction," Appl. Phys. Lett. **63**, 1214–1215 (1993).

[4]U. K. Mishra, P. Parikh, and Y.-F. Wu, "AlGaN/GaN HEMTs-an overview of device operation and applications," Proc. IEEE **90**, 1022–1031 (2002).

[5]S. Thompson, M. Armstrong, C. Auth, M. Alavi, M. Buehler, R. Chau, S. Cea, T. Ghani, G. Glass, T. Hoffman, C.-H. Jan, C. Kenyon, J. Klaus, K. Kuhn, Z. Ma, B. Mcintyre, K. Mistry, A. Murthy, B. Obradovic, R. Nagisetty, P. Nguyen, S. Sivakumar, R. Shaheed, L. Shifren, B. Tufts, S. Tyagi, M. Bohr, and Y. El-Mansy, "A 90-nm logic technology featuring strained-silicon," IEEE Trans. Electron Devices **51**, 1790–1797 (2004).

[6]H. W. Then, M. Radosavljevic, S. Bader, A. Zubair, H. Vora, N. Nair, P. Koirala, M. Beumer, P. Nordeen, A. Vyatskikh, T. Hoff, J. Peck, R. Nahm, T. Michaelos, E. Khora, R. Jordan, C. Hoffman, N. Franco, A. Oni, S. Beach, D. Garg, D. Frolov, A. Latorre-Rey, A. Mitaenko, J. Rangaswamy, S. Sarkar, S. Ahmed, V. Rayappa, H. Chiu, A. Hubert, S. Brophy, N. Arefm, N. Desai, H. Krishnamurthy, J. Yu, K. Ravichandran, and P. Fischer, "DrGaN: An integrated CMOS driver-GaN power switch technology on 300 mm GaN-on-Si with E-mode GaN MOSHEMT and 3D monolithic Si PMOS," in *International Electron Devices Meeting (IEDM)* (IEEE, 2023), pp. 1–4.

[7]H. W. Then, S. Dasgupta, M. Radosavljevic, P. Agababov, I. Ban, R. Bristol, M. Chandhok, S. Chouksey, B. Holybee, C. Y. Huang, B. Krist, K. Jun, K. Lin, N. Nidhi, T. Michaelos, B. Mueller, R. Paul, J. Peck, W. Rachmady, D. Staines, T. Talukdar, N. Thomas, T. Tronic, P. Fischer, and W. Hafez, "3D heterogeneous integration of high performance high-K metal gate GaN NMOS and Si PMOS transistors on 300 mm high-resistivity Si substrate for energy-efficient and compact power delivery, RF (5G and beyond) and SoC applications," in *IEEE International Electron Devices Meeting (IEDM)* (IEEE, 2019), pp. 17.3.1–17.3.4.

[8]N. Chowdhury, Q. Xie, M. Yuan, K. Cheng, H. W. Then, and T. Palacios, "Regrowth-free GaN-based complementary logic on a Si substrate," IEEE Electron Device Lett. **41**, 820–823 (2020).

[9]H. W. Then, M. Radosavljevic, P. Koirala, N. Thomas, N. Nair, I. Ban, T. Talukdar, P. Nordeen, S. Ghosh, S. Bader, T. Hoff, T. Michaelos, R. Nahm, M. Beumer, N. Desai, P. Wallace, V. Hadagali, H. Vora, A. Oni, X. Weng, K. Joshi, I. Meric, C. Nieva, S. Rami, and P. Fischer, "Advanced scaling of enhancement mode high-K gallium nitride-on-300 mm-Si(111) transistor and 3D layer transfer GaN-Silicon FinFET CMOS integration," in *IEEE International Electron Devices Meeting (IEDM)* (IEEE, 2021), pp. 11.1.1–11.1.4.

[10]H. W. Then, M. Radosavljevic, P. Koirala, M. Beumer, S. Bader, A. Zubair, T. Hoff, R. Jordan, T. Michaelos, J. Peck, I. Ban, N. Nair, H. Vora, K. Joshi, I. Meric, A. Oni, N. Desai, H. Krishnamurthy, K. Ravichandran, J. Yu, S. Beach, D. Frolov, A. Hubert, A. Latorre-Rey, S. Rami, J. Rangaswamy, Q. Yu, and P. Fischer, "Scaled submicron field-plated enhancement mode high-K gallium nitride transistors on 300 mm Si(111) wafer with power FoM (R_{ON}xQ_{GG}) of 3.1 mohm-nC at 40V and f_T/f_{MAX} of 130/680GHz," in *International Electron Devices Meeting (IEDM)* (IEEE, 2022), pp. 35.1.1–35.1.4.

[11]R. S. Pengelly, S. M. Wood, J. W. Milligan, S. T. Sheppard, and W. L. Pribble, "A review of GaN on SiC high electron-mobility power transistors and MMICs," IEEE Trans. Microwave Theory Tech. **60**, 1764–1783 (2012).

[12]J. Y. Tsao, S. Chowdhury, M. A. Hollis, D. Jena, N. M. Johnson, K. A. Jones, R. J. Kaplar, S. Rajan, C. G. Van De Walle, E. Bellotti, C. L. Chua, R. Collazo, M. E. Coltrin, J. A. Cooper, K. R. Evans, S. Graham, T. A. Grotjohn, E. R. Heller, M. Higashiwaki, M. S. Islam, P. W. Juodawlkis, M. A. Khan, A. D. Koehler, J. H. Leach, U. K. Mishra, R. J. Nemanich, R. C. N. Pilawa-Podgurski, J. B. Shealy, Z. Sitar, M. J. Tadjer, A. F. Witulski, M. Wraback, and J. A. Simmons, "Ultrawide-bandgap semiconductors: Research opportunities and challenges," Adv. Elect. Mater. **4**, 1600501 (2018).

[13]M. Rosker, C. Bozada, H. Dietrich, A. Hung, D. Via, S. Binari, E. Vivierios, E. Cohen, and J. Hodiak, "The DARPA wide band gap semiconductors for RF applications (WBGS-RF) program: Phase II results," CS ManTech **1**, 1–4 (2009).

[14]N. Islam, M. F. P. Mohamed, M. F. A. J. Khan, S. Falina, H. Kawarada, and M. Syamsul, "Reliability, applications and challenges of GaN HEMT technology for modern power devices: A review," Crystals **12**, 1581 (2022).

[15]D. Jena, *Quantum Physics of Semiconductor Materials and Devices* (Oxford University Press, 2022).

[16]S. Salahuddin, K. Ni, and S. Datta, "The era of hyper-scaling in electronics," Nat. Electron. **1**, 442–450 (2018).

[17]T. S. Böscke, J. Müller, D. Bräuhaus, U. Schröder, and U. Böttger, "Ferroelectricity in hafnium oxide thin films," Appl. Phys. Lett. **99**, 102903 (2011).

[18]C. P. Savant, C.-M. Tsai, and T.-W. Yu, "Dopant profile control in gate structures for semiconductor devices," USPTO Patent US20220336289A1 (2022).

[19]S. Fichtner, N. Wolff, F. Lofink, L. Kienle, and B. Wagner, "AlScN: A III-V semiconductor based ferroelectric," J. Appl. Phys. **125**, 114103 (2019).

[20]J. Casamento, H. Lee, T. Maeda, V. Gund, K. Nomoto, L. van Deurzen, W. Turner, P. Fay, S. Mu, C. G. Van de Walle *et al.*, "Epitaxial $Sc_xAl_{1-x}N$ on GaN exhibits attractive high-k dielectric properties," Appl. Phys. Lett. **120**, 152901 (2022).

[21]L. van Deurzen, T.-S. Nguyen, J. Casamento, H. Xing, and D. Jena, "Epitaxial lattice-matched AlScN/GaN distributed Bragg reflectors," Appl. Phys. Lett. **123**, 241104 (2023).

[22]T.-S. Nguyen, N. Pieczulewski, C. Savant, J. J. P. Cooper, J. Casamento, R. S. Goldman, D. A. Muller, H. G. Xing, and D. Jena, "Lattice-matched multiple channel AlScN/GaN heterostructures," APL Mater. **12**, 101117 (2024).

[23]D. V. Dinh, J. Lähnemann, L. Geelhaar, and O. Brandt, "Lattice parameters of $Sc_xAl_{1-x}N$ layers grown on GaN (0001) by plasma-assisted molecular beam epitaxy," Appl. Phys. Lett. **122**, 152103 (2023).

[24]A. J. Green, J. K. Gillespie, R. C. Fitch, D. E. Walker, M. Lindquist, A. Crespo, D. Brooks, E. Beam, A. Xie, V. Kumar, J. Jimenez, C. Lee, Y. Cao, K. D. Chabak, and G. H. Jessen, "ScAlN/GaN high-electron-mobility transistors with 2.4-A/mm current density and 0.67-S/mm transconductance," IEEE Electron Device Lett. **40**, 1056–1059 (2019).

[25]T. E. Kazior, E. M. Chumbes, B. Schultz, J. Logan, D. J. Meyer, and M. T. Hardy, "High power density ScAlN-Based heterostructure FETs for mm-wave applications," in *IEEE MTT-S International Microwave Symposium (IMS)* (IEEE, Boston, MA, 2019) pp. 1136–1139.

[26]J. Casamento, T.-S. Nguyen, Y. Cho, C. Savant, T. Vasen, S. Afroz, D. Hannan, H. G. Xing, and D. Jena, "Transport properties of polarization-induced 2D electron gases in epitaxial AlScN/GaN heterojunctions," Appl. Phys. Lett. **121**, 192101 (2022).

[27]J. Casamento, K. Nomoto, T. Nguyen, H. Lee, C. Savant, L. Li, A. Hickman, T. Maeda, J. Encomendero, V. Gund *et al.*, "FerroHEMTs: High-current and high-speed all-epitaxial AlScN/GaN ferroelectric transistors," in *International Electron Devices Meeting (IEDM)* (IEEE, 2022), pp. 11.1.

[28]J. Casamento, K. Nomoto, T.-S. Nguyen, H. Lee, C. Savant, L. Li, A. Hickman, T. Maeda, Y.-T. Shao, J. Encomendero, V. Gund, T. Vasen, S. Afroz, D. Hannan, D. A. Muller, H. G. Xing, and D. Jena, "AlScN high electron mobility transistors: Integrating high piezoelectric, high K dielectric, and ferroelectric functionality," in *IEEE BiCMOS and Compound Semiconductor Integrated Circuits and Technology Symposium (BCICTS)* (IEEE, 2023), pp. 132–136.

[29]J. Casamento, H. G. Xing, and D. Jena, "Oxygen incorporation in the molecular beam epitaxy growth of $Sc_xGa_{1-x}N$ and $Sc_xAl_{1-x}N$," Phys. Status Solidi B **257**, 1900612 (2020).

[30]N. N. Greenwood and A. Earnshaw, "Chemistry of the elements, chapter 20: Scandium, yttrium, lanthanum and actinium," in *Chemistry of the Elements* (Butterworth-Heinemann, 1997), Vol. 2, pp. 944–953.

[31]M. Baeumler, Y. Lu, N. Kurz, L. Kirste, M. Prescher, T. Christoph, J. Wagner, A. Žukauskaitė, and O. Ambacher, "Optical constants and band gap of wurtzite

$Al_{1-x}Sc_xN/Al_2O_3$ prepared by magnetron sputter epitaxy for scandium concentrations up to x= 0.41," J. Appl. Phys. **126**, 045715 (2019).
[32]J. Hayden, M. D. Hossain, Y. Xiong, K. Ferri, W. Zhu, M. V. Imperatore, N. Giebink, S. Trolier-McKinstry, I. Dabo, and J.-P. Maria, "Ferroelectricity in boron-substituted aluminum nitride thin films," Phys. Rev. Mater. **5**, 044412 (2021).
[33]S. Calderon, J. Hayden, S. M. Baksa, W. Tzou, S. Trolier-McKinstry, I. Dabo, J.-P. Maria, and E. C. Dickey, "Atomic-scale polarization switching in wurtzite ferroelectrics," Science **380**, 1034–1038 (2023).
[34]C. Savant, V. Gund, K. Nomoto, T. Maeda, S. Jadhav, J. Lee, M. Ramesh, E. Kim, T.-S. Nguyen, Y.-H. Chen *et al.*, "Ferroelectric AlBN films by molecular beam epitaxy," Appl. Phys. Lett. **125**, 072902 (2024).
[35]C. Savant, T.-S. Nguyen, S. Vishwakarma, J. Lee, A. Ithepalli, Y.-H. Chen, K. Nomoto, F. Rana, D. J. Smith, H. G. Xing *et al.*, "Epitaxial AlBN/β-Nb_2N ferroelectric/superconductor heterostructures," Phys. Status Solidi RRL **18**, 2400157 (2024).
[36]W. Hoke, A. Torabi, R. Hallock, J. Mosca, and T. Kennedy, "Reaction of molecular beam epitaxial grown AlN nucleation layers with SiC substrates," J. Vac. Sci., Technol. B **24**, 1500–1504 (2006).
[37]W. Hoke, A. Torabi, J. Mosca, and T. Kennedy, "Thermodynamic analysis of cation incorporation during molecular beam epitaxy of nitride films using metal-rich growth conditions," J. Vac. Sci. Technol., B **25**, 978–982 (2007).
[38]H. Lu, B. Hou, L. Yang, F. Song, M. Zhang, M. Wu, X. Ma, and Y. Hao, "Low-resistance Ta/Al/Ni/Au ohmic contact and formation mechanism on AlN/GaN HEMT," IEEE Trans. Electron Devices **69**, 6023–6027 (2022).
[39]H. Blanck, "Electrical properties, microstructure, and thermal stability of Ta-based ohmic contacts annealed at low temperature for GaN HEMTs," Semicond. Sci. Technol. **26**, 075006 (2011).
[40]J. Ben, X. Sun, Y. Jia, K. Jiang, Z. Shi, H. Liu, Y. Wang, C. Kai, Y. Wu, and D. Li, "Defect evolution in AlN templates on PVD-AlN/sapphire substrates by thermal annealing," CrystEngComm **20**, 4623–4629 (2018).
[41]M. Biswas, "Impact of annealing temperature on structural, electrical and optical properties of epitaxial GaN thin films grown on sapphire substrates by PA-MBE," arXiv:1509.00416 (2015).
[42]S. H. Chan, S. Keller, M. Tahhan, H. Li, B. Romanczyk, S. P. DenBaars, and U. K. Mishra, "High electron mobility recovery in AlGaN/GaN 2DEG channels regrown on etched surfaces," Semicond. Sci. Technol. **31**, 065008 (2016).
[43]G. Snider, see https://www3.nd.edu/gsnider/ for "1D poisson solver."
[44]K. Liu, H. Sun, F. AlQatari, W. Guo, X. Liu, J. Li, C. G. Torres Castanedo, and X. Li, "Wurtzite BAlN and BGaN alloys for heterointerface polarization engineering," Appl. Phys. Lett. **111**, 222106 (2017).
[45]C. L. Milne, T. Biswas, and A. K. Singh, "Electronic properties of $B_xAl_{1-x}N$ computed from GW simulations," arXiv:2309.16050 (2023).
[46]W. Nunn, T. K. Truttmann, and B. Jalan, "A review of molecular-beam epitaxy of wide bandgap complex oxide semiconductors," J. Mater. Res. **36**, 4846 (2021).
[47]D. Wang, S. Mondal, J. Liu, M. Hu, P. Wang, S. Yang, D. Wang, Y. Xiao, Y. Wu, T. Ma *et al.*, "Ferroelectric YAlN grown by molecular beam epitaxy," Appl. Phys. Lett. **123**, 033504 (2023).
[48]A. Rowberg, S. Mu, M. Swift, and C. Van de Walle, "Structural, electronic, and polarization properties of YN and LaN," Phys. Rev. Mater. **5**, 094602 (2021).
[49]Y. Utsumi, T. Imai, and N. Fujimori, "Boron-aluminum nitride coating and method of producing same," USPTO Patent US5766783 (1998).
[50]R. Kudrawiec and D. Hommel, "Bandgap engineering in III-nitrides with boron and group V elements: Toward applications in ultraviolet emitters," Appl. Phys. Rev. **7**, 041314 (2020).
[51]J.-X. Shen, D. Wickramaratne, and C. G. Van de Walle, "Band bowing and the direct-to-indirect crossover in random BAlN alloys," Phys. Rev. Mater. **1**, 065001 (2017).
[52]A. Suceava, J. Hayden, K. P. Kelley, Y. Xiong, B. Fazlioglu-Yalcin, I. Dabo, S. Trolier-McKinstry, J.-P. Maria, and V. Gopalan, "Enhancement of second-order optical nonlinearities and nanoscale periodic domain patterning in ferroelectric boron-substituted aluminum nitride thin films," Opt. Mater. Express **13**, 1522–1534 (2023).
[53]C. Savant, K. Nomoto, T.-S. Nguyen, Y.-H. Chen, R. Page, J. Casamento, Y. Cho, H. G. Xing, and D. Jena, "MBE growth, characterization of AlBN films and 2D electron gas in epitaxial AlBN/GaN heterojunction," in *Electronic Materials Conference* (Underline Science Inc, 2023).
[54]A. R. Smith, H. A. Al-Brithen, D. C. Ingram, and D. Gall, "Molecular beam epitaxy control of the structural, optical, and electronic properties of ScN (001)," J. Appl. Phys. **90**, 1809–1816 (2001).
[55]B. Saha, J. Acharya, T. D. Sands, and U. V. Waghmare, "Electronic structure, phonons, and thermal properties of ScN, ZrN, and HfN: A first-principles study," J. Appl. Phys. **107**, 033715 (2010).
[56]M. J. Winiarski and D. Kowalska, "Electronic structure of REN (RE= Sc, Y, La, and Lu) semiconductors by MBJLDA calculations," Mater. Res. Express **6**(9), 095910 (1997).
[57]M. J. Winiarski and D. A. Kowalska, "Crystal structure of rare earth and group III nitride alloys by ab initio calculations," Sci. Rep. **10**, 16414 (2020).
[58]P. Larson, W. R. L. Lambrecht, A. Chantis, and M. Van Schilfgaarde, "Electronic structure of rare-earth nitrides using the LSDA + U approach: Importance of allowing 4f orbitals to break the cubic crystal symmetry," Phys. Rev. B **75**, 045114 (2007).
[59]S. Leone, I. Streicher, M. Prescher, P. Straňák, and L. Kirste, "Metal-organic chemical vapor deposition of aluminum yttrium nitride," Phys. Status Solidi RRL **17**, 2300091 (2023).
[60]P. Wang, D. Wang, S. Mondal, M. Hu, J. Liu, and Z. Mi, "Dawn of nitride ferroelectric semiconductors: From materials to devices," Semicond. Sci. Technol. **38**, 043002 (2023b).
[61]G. A. Alvarez, J. Casamento, L. van Deurzen, M. I. Khan, K. Khan, E. Jeong, E. Ahmadi, H. G. Xing, D. Jena, and Z. Tian, "Thermal conductivity enhancement of aluminum scandium nitride grown by molecular beam epitaxy," Mater. Res. Lett. **11**, 1048 (2023).
[62]D. Jena, R. Page, J. Casamento, P. Dang, J. Singhal, Z. Zhang, J. Wright, G. Khalsa, Y. Cho, and H. G. Xing, "The new nitrides: Layered, ferroelectric, magnetic, metallic and superconducting nitrides to boost the GaN photonics and electronics eco-system," Jpn. J. Appl. Phys., Part 1 **58**, SC0801 (2019).